Computer-Aided Phase Shift Mask Design with Reduced Complexity

Yong Liu, *Member, IEEE*, Avideh Zakhor, and Marco A. Zuniga

Abstract— We propose a new approach to systematic phase shift mask design. In doing so, we constrain the complexity of the mask at a pre-specified level by limiting the number of "features" on the mask. We then optimize the location, size and phase of the features so as to achieve a desired intensity pattern on the wafer. The main advantage of this object-based approach over our previous pixel-based solution is that it results in substantially larger assisting phase shift features, and is therefore easier to fabricate. Our approach can also be used to design masks with proper bias and/or extension of the depth of focus. We will show examples of contact hole, bright line and chromeless line-space mask designs. Finally we show experimental results using the new approach.

I. INTRODUCTION

SINCE the revitalization of phase shift mask technology, computer-aided interactive design tools have been developed to allow extraction of image quality information and bloating or shifting of a particular feature [1]. While these tools provide user friendly environments for design engineers, new phase shift configurations have to be conceived either by highly experienced engineers or through extensive trial and error. Our previously proposed systematic mask design technique on the other hand, allows automation of the above process by optimizing mask patterns numerically, thus avoiding trial and error [2], [3]. Specifically, the bit-map based optimization algorithm in [2] and [3] is based on the Simulated Annealing (SA) algorithm: given a specification of a desired output light intensity at certain range of defocus, the algorithm chooses a nearly optimal bit-map mask pattern according to a chosen criterion. The designed masks have excellent performance, but are complex with many small pixels scattered around the main features.

In this paper, we move one step closer to the systematic design of *practical* phase shift masks by taking a new approach based on the algorithm in [2] and [3]. This new approach can be used to design masks with reduced complexity, suitable for high volume manufacturing environments. Specifically, we view a mask as a collection of objects, with their locations, sizes, transmission coefficients and phases to be determined. In doing so, we are able to design masks with pre-specified complexity, where by complexity we mean the number of

Y. Liu is with CIDA Technology, Inc., Sunnyvale, CA 94086 USA.
A. Zakhor and M. Zuniga are with the Department of Electrical Engineering and Computer Sciences, University of California, Berkeley, CA 94720 USA.
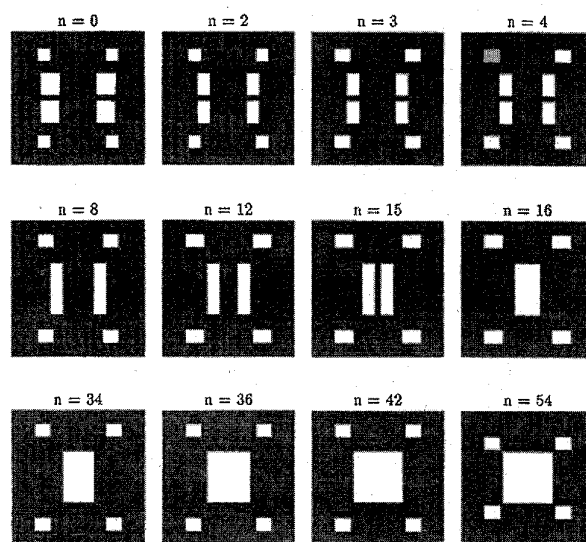
Fig. 1. The evolution of a mask pattern, during the optimization by bacteria algorithm, at steps 0, 2, 3, 4, 8, 12, 15, 16, 34, 36, 42, 54.

objects allowed and the minimum object size. The objects can be arbitrary rectangles with dimensions larger than the minimum feature size, and with a phase chosen from a finite size set of discrete phases. The positioning of the objects is at a finer resolution than the minimum feature size, for example at 1/4 of the minimum feature size. This reflects the fine positioning capability of the mask-making machine and results in increased flexibility in the optimization process, thus compensating for the loss of freedom due to limited number of objects and a larger minimum feature size. Therefore, masks designed by this new approach are likely to maintain the performance we previously achieved in [2] and [3] while being considerably more practical for manufacturing purposes.

Unlike the approach in [2] and [3], where the pixels have fixed sizes at fixed locations, our new approach allows each object to expand or contract and change positions. Each such change generates a new mask to be evaluated. To facilitate this generation process within the previously stated constraints, we propose to use what we call the "bacteria" algorithm. This algorithm allows a randomly chosen object to change its position, left, right, up and down, or to expand/contract on a certain edge to the left, right, up or down. The algorithm employs the strategy of a bacteria in search of its food to govern the process of generating and accepting/rejecting new masks. It can quickly lead the search to a local minimum, even
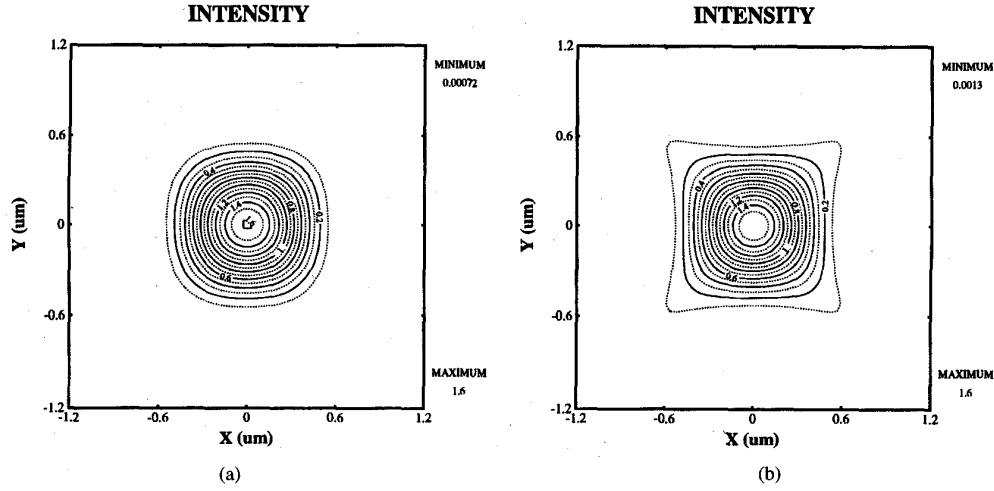
Fig. 2. Intensity distributions at the focus plane due to, (a) a conventional binary mask without serif, (b) the designed mask in Fig. 1 with serif.
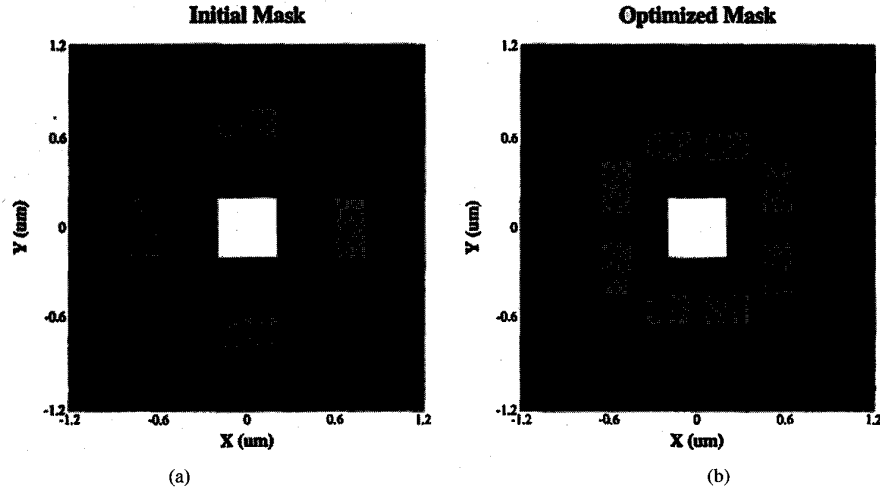

Fig. 3. (a) Initial and (b) optimized phase shift masks for a 0.4 μm contact hole, where the dark area is opaque; all the other areas are transparent with different phases: white for $0°$, shade for $180°$.

though it needs to be modified in order to find a near-global minimum.

The outline of this paper is as follows. In Section II, we describe the problem formulation and the solution space. In Section III, we present our proposed bacteria algorithm and its variants. In Section IV, we show masks designed by this approach which can provide a proper bias and extend the depth of focus. In Section V, we verify the usefulness of the new approach by doing experiment with the newly designed masks. Conclusions and suggestions for future research directions are discussed in Section VI.

II. PROBLEM FORMULATION

For convenience, we consider a rectangular field of interest $(0, l_x) \times (0, l_y)$ as the mask area to be optimized. A mask is considered to be a collection of geometric objects with certain sizes, levels and locations in this field. Each level consists of a transmission coefficient and a phase. In practice,

there are a finite number of transmission coefficients and phases. Since the transmission coefficient is typically either 0 or 1 and fixed, we will use the words "level" and "phase" interchangeably. We allow two classes of objects in the mask. One class is composed of fixed objects, which represent the environment under which our optimization is performed and are therefore not modified during the optimization process. These objects can be any polygon at any location and with any available level. The second class of objects is composed of variable or floating objects, whose sizes, locations and levels are to be determined during the optimization process. For convenience, we only consider *rectangular* floating objects. To be manufacturable, the sizes of all objects must be larger than the minimum mask feature size Δ. The location of a floating object is on a discrete grid where the grid size δ is smaller than the minimum feature size. For example, the grid size can be four times smaller than minimum feature size, i.e., $\Delta = 4 \times \delta$, to reflect the capability of a mask-making
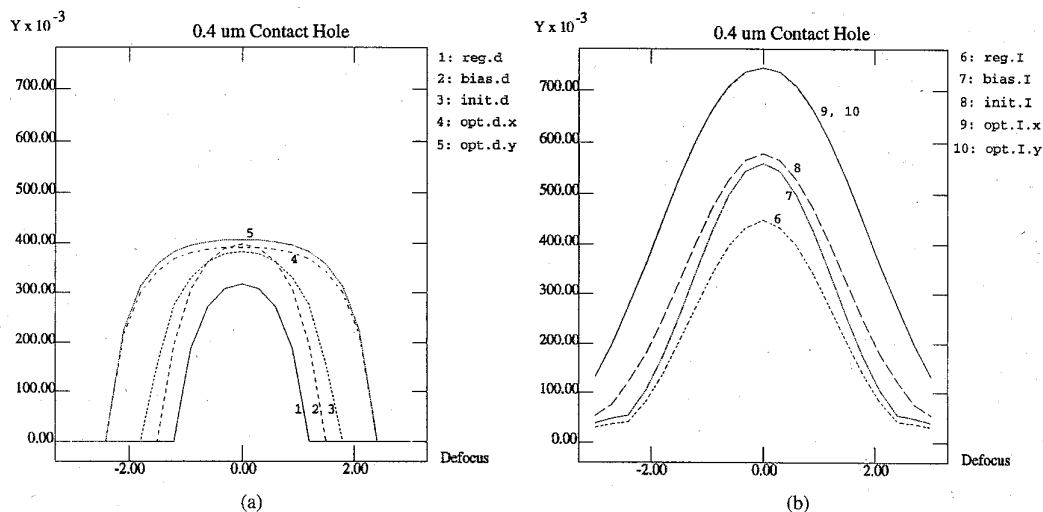
Fig. 4. (a) Contact hole diameter and (b) maximum intensity of the mask in Fig. 3(b), at different optical planes due to different masks with the following notations: "d" for contact hole diameter, "I" for maximum intensity, "reg" for 0.4 μm conventional binary mask, "bias" for 0.432 μm biased binary mask, "init" for initial mask of the optimization, "opt" for optimized mask, "x" for the x-direction, "y" for the y-direction.
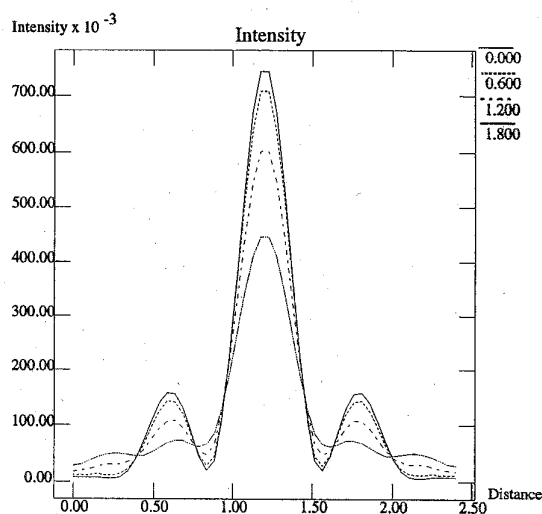

Fig. 5. Intensity distribution along the y direction at different optical planes due to the mask in Fig. 3(b).
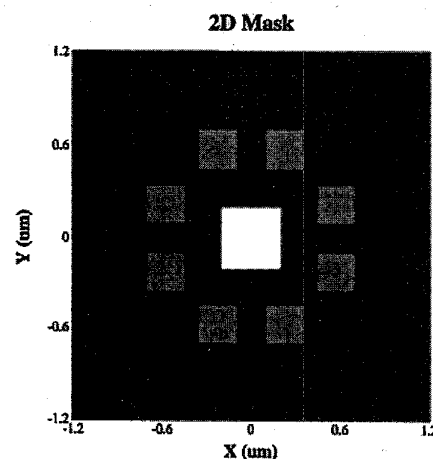

Fig. 6. The initial mask, obtained by manually modifying the mask in Fig. 3(b). The optimization starting from this mask results in the optimized mask in Fig. 7(a). In the mask, the dark area is opaque; all the other areas are transparent with different phases: white for 0°, shade for 180°.

machine. To avoid the formation of features smaller than Δ, no object is allowed to overlap with any other object during the optimization process.

Clearly, if we do not limit the number of objects in the optimization process, then given a minimum mask feature size, the solution space for bit-map based approach becomes a subset of the solution space of object-based approach. Intuitively, the size of this subset is much smaller than the size of its superset, the solution space of the object-based approach. In general however, it is hard to compare the size of these two spaces if the number of objects is limited. This is due to the difficulty in counting all the possible positions and sizes of each object in the object-based approach.

Taking advantage of the increase in solution space, it is conceivable to use a larger minimum feature size in the object-based mask optimization and simultaneously maintain the

same performance as a bit-map based mask. This possibility is justified because the relative positioning of the mask features influences the nature of the light interference pattern, while the size of the features only influences the strength of the light interference. Since our proposed object-based approach can position objects at a finer resolution than minimum feature size, we can still control the light interference pattern in order to arrive at masks with acceptable performance and yet practical for manufacturing purposes.

III. THE BACTERIA ALGORITHM

In this section, we assume that given any mask, we can calculate the resulting intensity $I(x, y)$ on a wafer at different optical planes. We also assume that we have a criterion $f(I)$ that evaluates the performance of a mask by comparing its intensity to a desired intensity pattern on the wafer [2], [3]. The
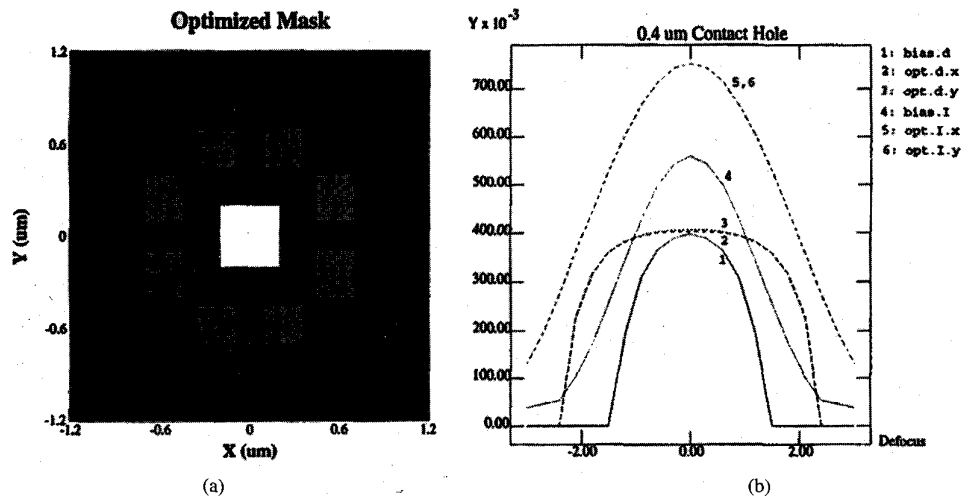
Fig. 7. (a) An almost symmetric optimized phase shift mask for 0.4 μm contact hole, where the dark area is opaque; all the other areas are transparent with different phases: white for 0°, shade for 180°. (b) Comparison of the contact hole diameter and the maximum intensity at different optical planes due to different masks with the following notations: "*d*" for contact hole diameter, "*I*" for maximum intensity, "bias" for 0.432 μm biased binary mask, "opt" for optimized mask, "*x*" for the *x*-direction and "*y*" for the *y*-direction.

optimization process is assumed to be iterative in nature. Given any initial mask, we generate a new mask by a generation rule, evaluate its performance by computing f, then decide whether to accept the new mask using an acceptance rule. We will repeat the above process until it terminates according to a stopping rule.

Due to the size of the solution space in the optimization process, the simulated annealing algorithm used in [2], [3] requires long time in order to obtain near-global optima. Therefore, we have opted to use a "bacteria algorithm", to efficiently find a local minimum. A bacteria does not have eyes, but it can still find places where there is a high concentration of food. The strategy it uses is simple: it randomly starts moving in a direction, tasting the food concentration along the way, and continues going in the same direction if the food concentration increases. When the food concentration decreases, the bacteria stops, randomly generates a new direction and repeats the above process. This way a bacteria always moves from low to high food concentration regions. In our search for the best mask given an arbitrary desired intensity pattern, we are in a similar position to a bacteria in its search of food. There is no easy way to know the way the objective function varies with the changes in the mask unless we actually compute the objective function. In contrast to the movement of a bacteria, we consider the direction that a mask "moves", in its solution space, to consist of a particular object in the mask being chosen, the chosen phase of the object, the direction of displacement of the object (left, right, up and down) or the expansion (contraction) of the object on a certain edge (left, right, up and down). There are two classes of movements to be distinguished. We define the movement of an object to be any displacement of its position or change of its size, but not the change of its phase. We define the movement of a mask to be any movement or change of phase of an object in the mask. Therefore, movement of an object always results in a movement of the mask, but not vice versa. Since changing

the phases of the objects affects optical interference in a more dramatic way than changing the positions and sizes of the objects, phase changes are restricted during the optimization. To save computation time, we set a low probability for the mask to move in a direction that requires a change of phase of an object. All the movement directions of an object are equally likely to be chosen. In each step of the optimization, the amount of displacement or change of size of an object is the grid size δ. The algorithm can be briefly described as follows.

1) Start with an initial mask which could either be random or designed in a specific way. Mark the mask movements in all directions as having been rejected.

2) Randomly choose a floating object.

3) Choose to modify the object by the following steps:

   a) If the last movement of the mask due to a movement of this object resulted in an acceptance of the new mask, then choose to move the object in the same direction as in the last movement.

   b) Otherwise, randomly choose a new movement direction for the object.

   If the previous movement of the object in the same direction resulted in an acceptance of the movement, then use this direction;

   else, flip a biased coin. With a small probability, choose to change the phase of the object and with a large probability, use the newly generated direction.

   c) If the chosen movement causes the chosen object to be outside optimization boundary, or to overlap with other fixed or floating objects, or to become smaller than the minimum feature size, then go back to step b.

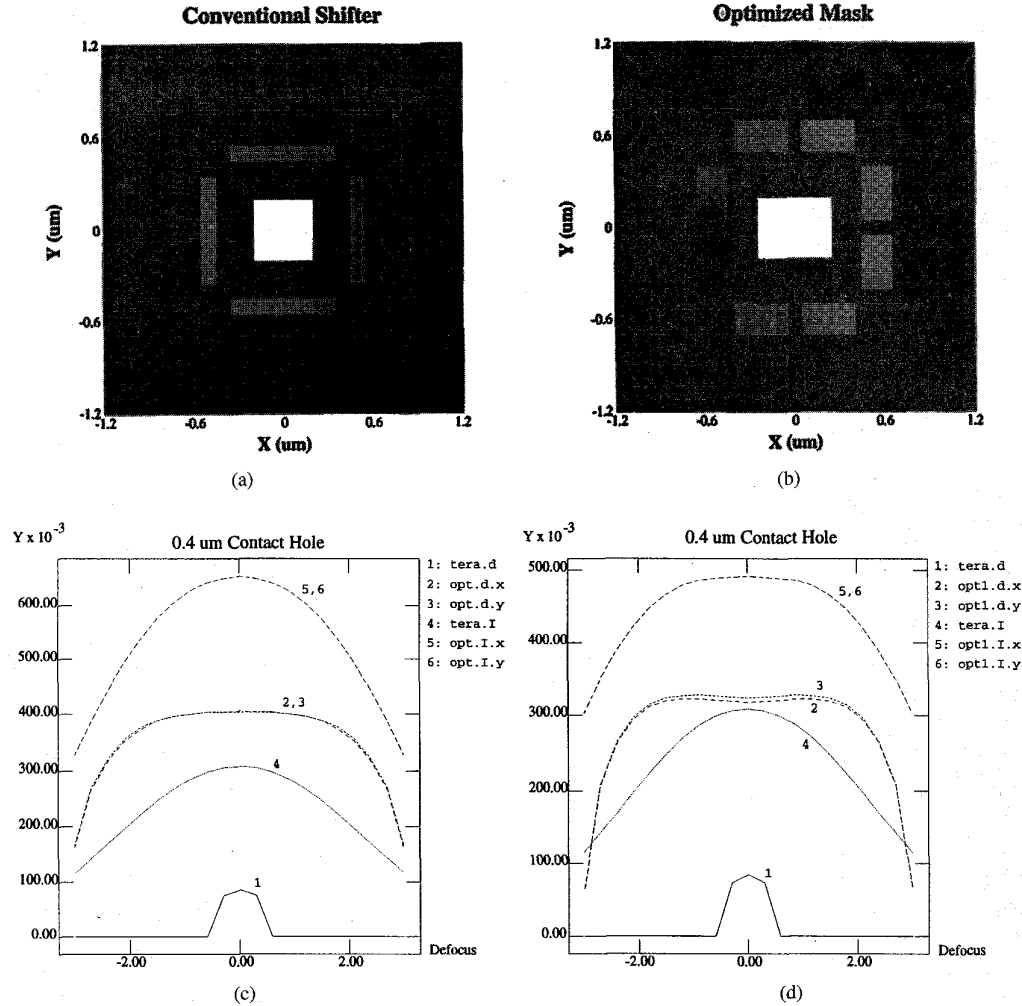4) Compute $f(I(x, y))$ due to the newly generated mask and compare it to the previous mask.

Fig. 8.   (a) Conventional outrigger mask design suggested in [7] and [8] and (b) our optimized phase shift mask design for a 0.4 μm contact hole, where the dark area is opaque; all the other areas are transparent with different phases: white for $0°$, shade for $180°$. (c), (d) Comparison of the contact hole diameter and the maximum intensity at different optical planes due to different masks with the following notations: "d" for contact hole diameter, "I" for maximum intensity, "tera" for conventional mask in (a), "opt1" for optimized mask in Fig. 7(a), "opt" for optimized mask in (b), "x" for the x-direction and "y" for the y-direction.

If f decreases, then accept the new mask and mark the direction as "accepted";

else, reject the new mask and mark the corresponding direction as "rejected".

5) Check the stopping rule; if not satisfied, go to step 2; otherwise stop and take the current mask as the optimized one. The stopping rule we have chosen is similar to that in [3].

This bacteria algorithm is effective in searching for a local minima, but not necessarily a good local minimum. The reasons are: (1) only a local search is conducted in each iterative step; (2) the acceptance rule is greedy. These two factors combined can produce the so called "infeasible direction", which happens when the edges of two floating objects are touching each other, and therefore can not move toward one another due to the no overlap constraint. If neither of the two objects can move away from each other due to the greedy acceptance rule, then there is no way to reach a mask which requires the boundary of the two objects to move simultaneously in a certain direction. In other words, the solution space in this algorithm is not connected.

The SA algorithm can be combined with the bacteria algorithm to overcome these problems, but our experience shows that due to the nature of the problem, the SA algorithm converges at an impractically slow rate. To allow efficient search of minima without falling into a shallow local minimum, we use a simple deterministic approach which more or less avoids shallow local minima. We simply calculate a moving average of the previous decreases of the objective function in single moves which were not necessarily accepted. The next move is accepted only if it results in a decrease of the objective function larger that a certain percentage of the moving average. This way, since the moving average decreases with iterations, major improvements are sought first, followed by minor improvements. This measure also helps to avoid the formation of infeasible directions due to movements with only a minor improvement. We have found experimentally that this
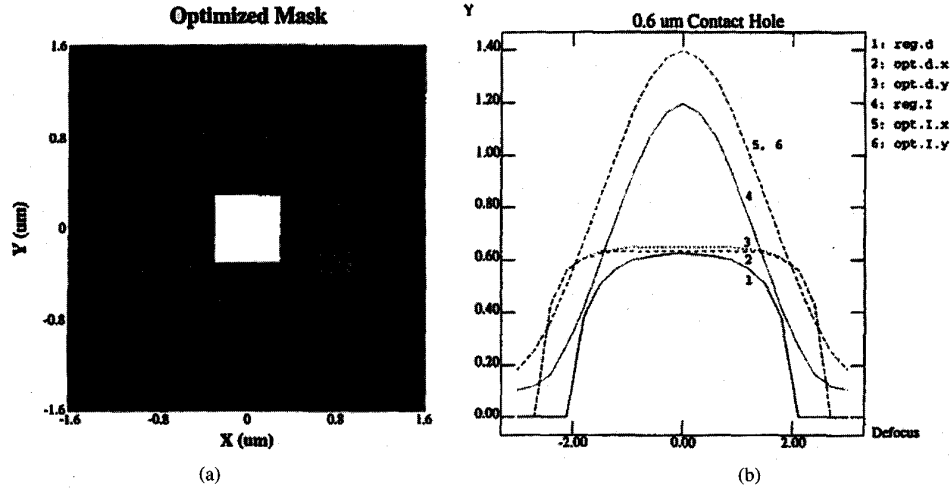
(a)   (b)

Fig. 9.   (a) An optimized phase shift mask for a 0.6 μm contact hole, where the dark area is opaque; all the other areas are transparent with different phases: white for 0°, shade for 180°. (b) Comparison of the contact hole diameter and the maximum intensity at different optical planes due to different masks with the following notations: "d" for contact hole diameter, "I" for maximum intensity, "reg" for conventional mask, "opt" for optimized mask, "x" for the x-direction and "y" for the y-direction.
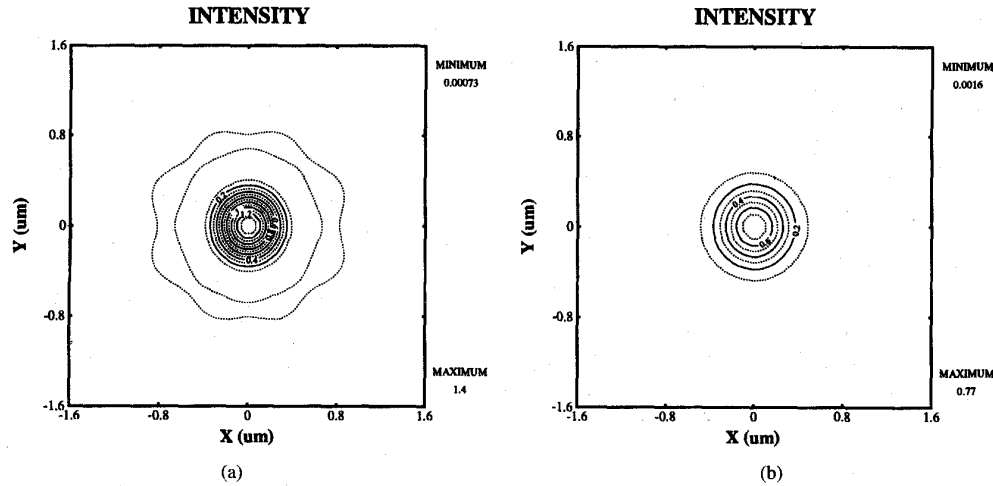

(a)   (b)

Fig. 10.   Contour plots for intensities at optical planes with (a) 0.0 μm and (b) 1.6 μm defocus, due to the optimized mask in Fig. 9(a).

measure causes the bacteria algorithm to converge at a slower rate but results in solutions of higher quality.

Finally, the bacteria algorithm performs well if the initial mask is near a "good" mask. Since its solutions do not deviate much from the initial mask, it is incapable of finding a near-global minimum. To facilitate the creation of new mask configurations, a different generation rule can be used in the beginning of the optimization. This rule allows the generation of objects with random size, location and phase, to replace an existing floating object. This way, the algorithm visits a larger portion of the solution space and is therefore more likely to find a near-global minimum than a local one.

IV. SIMULATION RESULTS

In all the examples in this section, the mask patterns are assumed to have four-fold symmetry. The optimization is done only to the first quadrant. All the simulations are done at i-line

(0.365 μm), 0.48 numerical aperture and 0.38 degree of partial coherence, unless otherwise stated. In all the mask patterns, the white areas represent transparent without any phase shift, dark shaded areas represent opaque areas and light shaded areas represent transparent areas with 180° phase shift. All the line widths on the wafer are calculated using a 0.3 contour size.

Fig. 1 shows the evolution of a binary mask pattern using the bacteria algorithm. The desired pattern is a 0.9 μm square. The optimization is done only at the focus plane. We have restricted the number of objects to two, the minimum mask feature size to $\Delta = 0.225$ μm and the grid resolution to $\delta = 0.056\,25$ μm. The optimization starts with two randomly generated rectangles in the first quadrant. One of the objects gradually evolves into a 0.9 μm square and the other object evolves into a serif at the proper position. Fig. 2 shows the intensity contours due to a conventional binary mask and the designed mask. Clearly, the serif compensates for optical diffraction at the corner, and the optimized mask results in
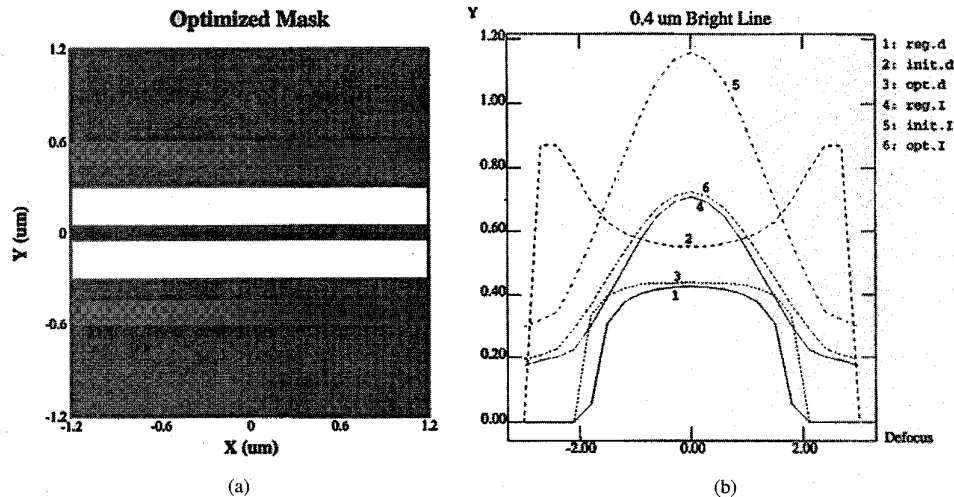
(a)   (b)

Fig. 11.   (a) An optimized phase shift mask for a 0.4 μm bright line or space, where the dark area is opaque; all the other areas are transparent with different phases: white for 0°, shade for 180°. (b) Comparison of the line width and the maximum intensity at different optical planes due to different masks with the following notations: "d" for line width, "I" for maximum intensity, "reg" for conventional binary mask, "init" for initial mask in the optimization, "opt" for optimized mask, "x" for the x-direction and "y" for the y-direction.

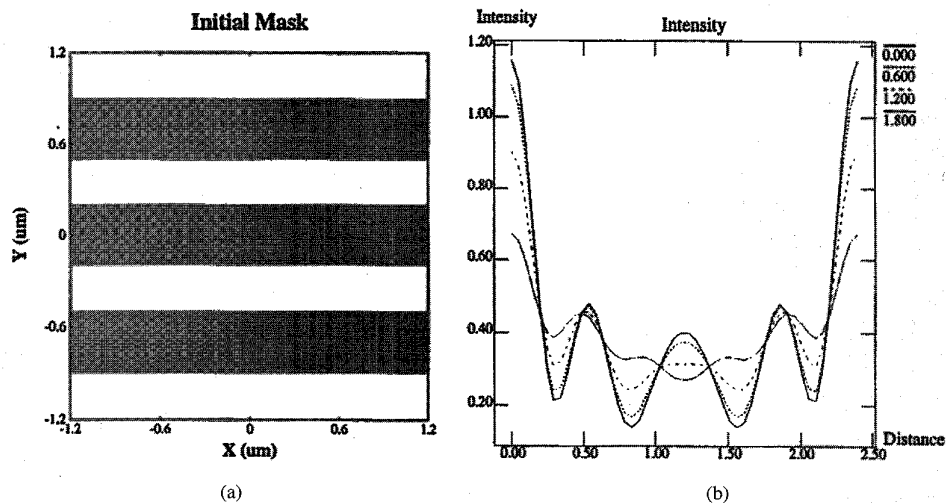(a)   (b)

Fig. 12.   (a) A guess of a chromeless mask with 0.4 μm lines and spaces, where all the areas are transparent with different phases: white for 0°, shade for 180°. (b) Maximum intensity along the y direction at different optical planes due to the initial mask in (a).

a more "squared" intensity pattern than that due to a mask without the serif. Of course, this is a special example in the sense that the resulting mask is already well known [4], [6]. Our second example deals with contact hole designs which are variations of outrigger and ring phase shift designs. The desired intensity pattern is a 0.4 μm contact hole at optical planes of 0 μm and 1.6 μm defocus. In the optimization, the minimum mask feature size is 0.2 μm $\times$ 0.2 μm and the positioning accuracy is 0.05 μm. The total number of objects is three, all of them floating objects. Starting with an arbitrarily constructed outrigger phase shift mask design, shown in Fig. 3(a), our algorithm produces the mask shown in Fig. 3(b). The performance of a conventional binary mask, its biased version with mask size 0.432 μm $\times$0.432 μm, the initial mask and the optimized mask are compared in Fig. 4. As seen,

the optimized phase shift mask not only provides the proper bias for the correct contact hole size, but also greatly extends the depth of focus, and enhances the contrast throughout the defocus range of interest. The extension of the depth of focus over a biased conventional mask is close to 200% and the enhancement of the contrast over a biased binary mask is about 35%.

One possible concern with the large phase shifters in the optimized design is the large side lobes. A plot of the intensity distribution along the y-axis, due to the mask in Fig. 3(b), is shown in Fig. 5. From this intensity plot, the largest side lobe occurs at the focus plane and is below 0.16. Since our specified threshold is 0.15, this side lobe can be considered acceptable. To obtain smaller side lobes, we can simply reduce the specified threshold in the optimization criteria [3]. We have
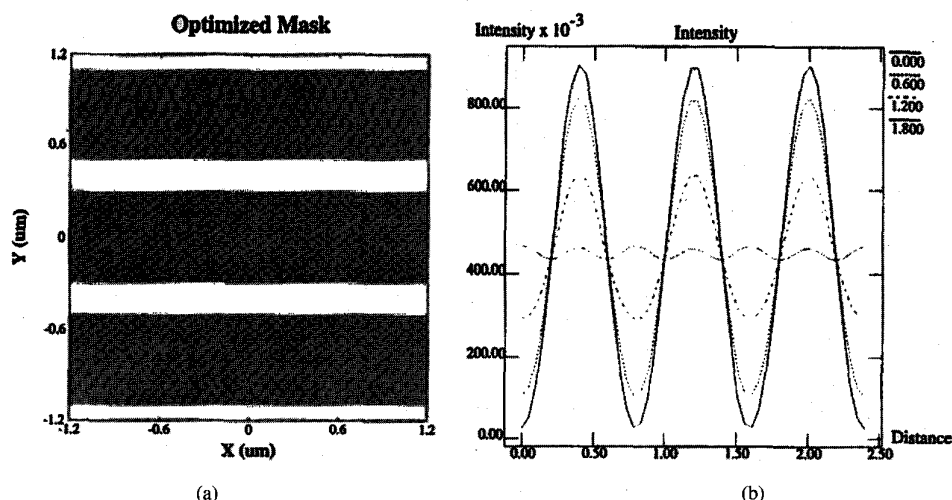
Fig. 13. (a) The optimized chromeless mask for 0.4 μm lines and spaces, where all the areas are transparent with different phases: white for 0°, shade for 180°. (b) Maximum intensity along the y direction at different optical planes due to the optimized mask in (a).

also found that the side lobes due to the mask in Fig. 3(b) are smaller in the x-direction than in y. Although the optimized mask is not symmetric with respect to the diagonal axis, the difference in line width in the x and y directions is only about 3%. We can manually modify the optimized mask in Fig. 3(b) to obtain a symmetric mask, shown in Fig. 6. Using this modified mask as an initial mask for the optimization process, we obtain an improved mask, shown in Fig. 7(a), whose line width is almost the same in the x and y directions, as shown in Fig. 7(b).

For comparison purposes, we have applied our algorithm to design a 0.4 μm contact hole for the same optical parameters used in [7] and [8], i.e., 0.42 numerical aperture and 0.3 degree of partial coherence. The mask in [7] and [8] and our designed mask are shown in Fig. 8(a) and (b) respectively, and their performance in terms of size and intensity is shown in Fig. 8(c). There are several advantages to our mask as compared to the one in [7] and [8]. First, unlike our designed mask in Fig. 8(b), the mask in [7] and [8] requires overexposure in order for it to result in a 0.4 μm contact hole; otherwise it results in a 0.1 μm contact hole as demonstrated in Fig. 8(c). Second, as seen in Fig. 8(c), the maximum intensity for our mask is at least 100% larger than that of the mask in [7] and [8]. Third, our designed mask has a longer depth of focus. Fourth, our designed mask is easier to fabricate because of larger phase shifter sizes.

The masks obtained via our object-based approach are not only easy to fabricate, but also robust. For example, if we use the contact hole mask shown in Fig. 7(a) with a different set of optical parameters than the ones it was designed for, its performance remains acceptable. Fig. 8(d) shows the contact hole size and maximum intensity due to the mask in Fig. 7(a) and the mask in [7] and [8]. As seen, the extension of depth of focus for our mask shown in Fig. 7(b) persists in Fig. 8(d), maintaining uniform contact hole size for about ±1.5 μm defocus. In addition, the maximum intensity of the mask in Fig. 7(a) is still larger than that of the mask in [7] and [8], even though it was optimized with a different set of optical parameters than it was tested with.

The new phase shift configurations presented in Figs. 3(b) and 7(a) are not unique to the 0.4 μm size. Optimizations for different contact hole sizes, such as 0.6 μm and 0.70 μm, have all resulted in similar configurations. We present an example which starts with a ring phase shift configuration, and converges to the configuration, shown in Fig. 9(a). The desired pattern is a 0.6 μm contact hole. The minimum mask feature size is again 0.2 μm $\times$ 0.2 μm, and the positioning accuracy is 0.05 μm. Although the mask is not identical to Figs. 3(b) and 7(a), the structure is inherently similar to the previously shown configurations, and its resulting intensity, shown in Fig. 10, is quite acceptable. Fig. 9(b) compares the line width and maximum intensity due to the designed mask and a binary conventional mask. The extension of the depth of focus and enhancement of the contrast are self-evident. This example indicates: (1) the shape of the assisting phase shifters is less important than the position and area of the phase shifters; (2) since starting with a ring phase shift design we arrive at a different configuration, we conclude that for contact holes, a ring phase shift design does not result in the best possible performance. Next we show an example of a space design. The desired pattern is a 0.4 μm space or bright line under the illumination of light with 0.58 degree of partial coherence. The optimization is done at 0.0 μm, and 1.5 μm defocus, with a minimum mask feature size of 1.2 μm $\times$ 0.1 μm and a positioning accuracy of 0.05 μm. The total number of objects is two, both floating objects. Starting from an outrigger type phase shift mask as the initial guess, the algorithm arrives at the mask shown in Fig. 11(a), which is a variation of the outrigger type mask. The line width and maximum intensity along different defocus due to the initial mask, the designed mask and a conventional binary mask are shown in Fig. 11(b). As seen, the initial mask produces a high intensity but incorrect line width (0.55 μm), the designed mask produces the correct line width and an extension of depth of focus without sacrificing the contrast, as compared with the conventional binary mask. An advantage of this designed mask over the one in [7], [8] is that, even though they have
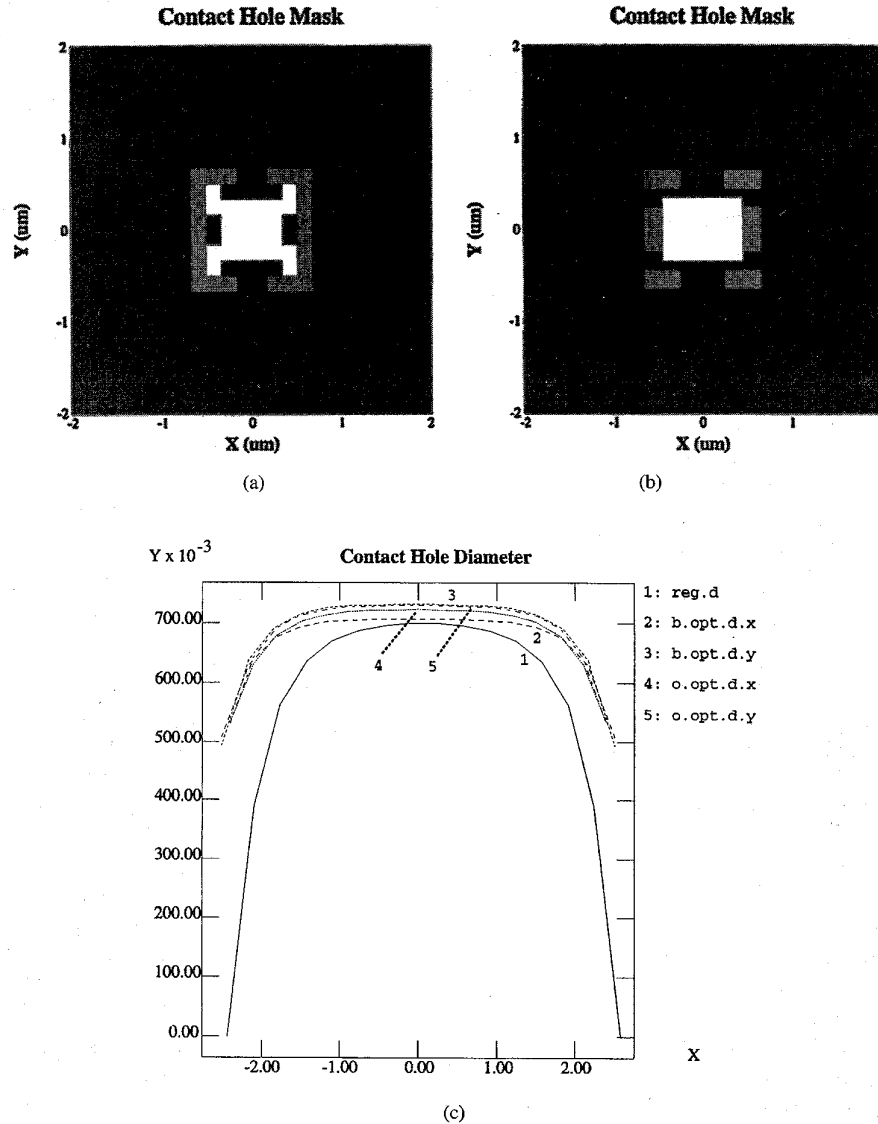
(a)

(b)

(c)

Fig. 14. Optimized masks based on bit-map mask (a) and object-based mask (b) for a 0.68 μm contact hole and their contact hole diameters (c). In the masks, the dark area is opaque; all other areas are transparent with different phases: white for $0°$, shade for $180°$. The notations in (c) are: "d" for contact hole diameter, "b" for bit-map based mask, "o" for object-based mask, "opt" for optimized mask, "reg" for conventional binary mask, "x" for the x-direction and "y" for the y-direction.

approximately the same performance, the phase shifter line width in our mask is 50% larger than that used in [7] and [8], and therefore easier to fabricate.

Next, we show an example of a chromeless phase shift mask design. The desired intensity pattern is composed of 0.4 μm equal lines and spaces. The degree of partial coherence is 0.58. The mask is optimized at 0.0 μm and 1.0 μm defocus. The optimization is done with two floating objects, a minimum feature size of 0.1 μ m$\times$0.1 μm and a positioning accuracy of 0.05 μm. We start with an initial mask in which line width of each phase region is equal to the desired line width, as shown in Fig. 12(a). The algorithm arrives at a mask, shown in Fig. 13(a), with the $180°$ phase shifter properly biased to give equal lines and spaces. The intensity distribution at different

optical planes due to the initial mask and our optimized mask are shown in Figs. 12(b) and 13(b), respectively. The initial mask has opposite phases with the same strength next to each other, cancelling out the light intensity. The optimized mask provides the proper biases for the $0°$ and $180°$ phases to enhance/suppress intensity at the proper places.

Finally, for comparison purposes, the pixel-based optimized mask in [3] and an object-based optimized mask for a 0.68 μm contact hole pattern are shown in Fig. 14(a) and (b), respectively. Both masks are optimized on 0.0 μm and 2.0 μm optical planes, at i-line with 0.45 numerical aperture and 0.5 degree of partial coherence. As seen in Fig. 14(c), their performance is nearly identical. But the object-based mask occupies less space, uses larger phase shifters and has simpler
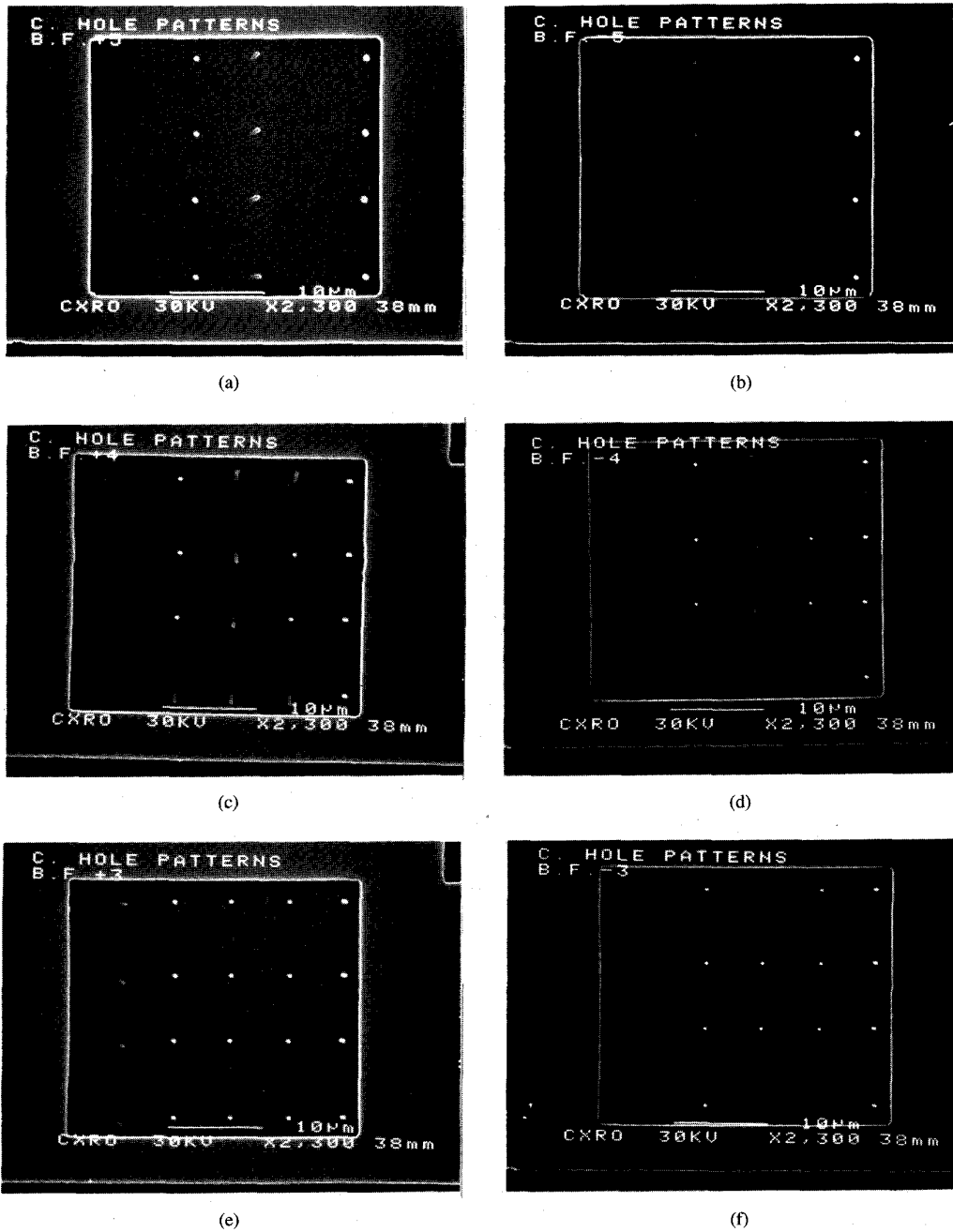
(a)

(b)

(c)

(d)

(e)

(f)

Fig. 15. SEM pictures of contact resist post images at different defocus planes, starting from +1 μm (top left) to −1 μm (top right) at increment of 0.2 μm. Each column in the SEM pictures correspond a particular design as described in Section V.

mask pattern than the bit-map based mask, and is therefore easier to fabricate. This example confirms our speculation in the introduction.

V. EXPERIMENTAL RESULTS

To verify the concepts proposed in this paper, experiments were carried out featuring contact holes designed using binary, conventional phase shift and our new approach. The phase shift masks were made using Cr on quartz, e.g., the phase shifters were made by etching proper amount on the quartz.

Negative resist (SNR248) was used so that posts rather than contact holes are obtained for the convenience of SEM picture taking. The exposure system had a wavelength of λ = 0.248 μm, numerical aperture of NA = 0.6 and degree of partial coherence of σ = 0.5. Standard process was used, i.e., best focus was determined by when the smallest line space pattern on a binary mask, which is 0.3 μm in size, prints well on the wafer.

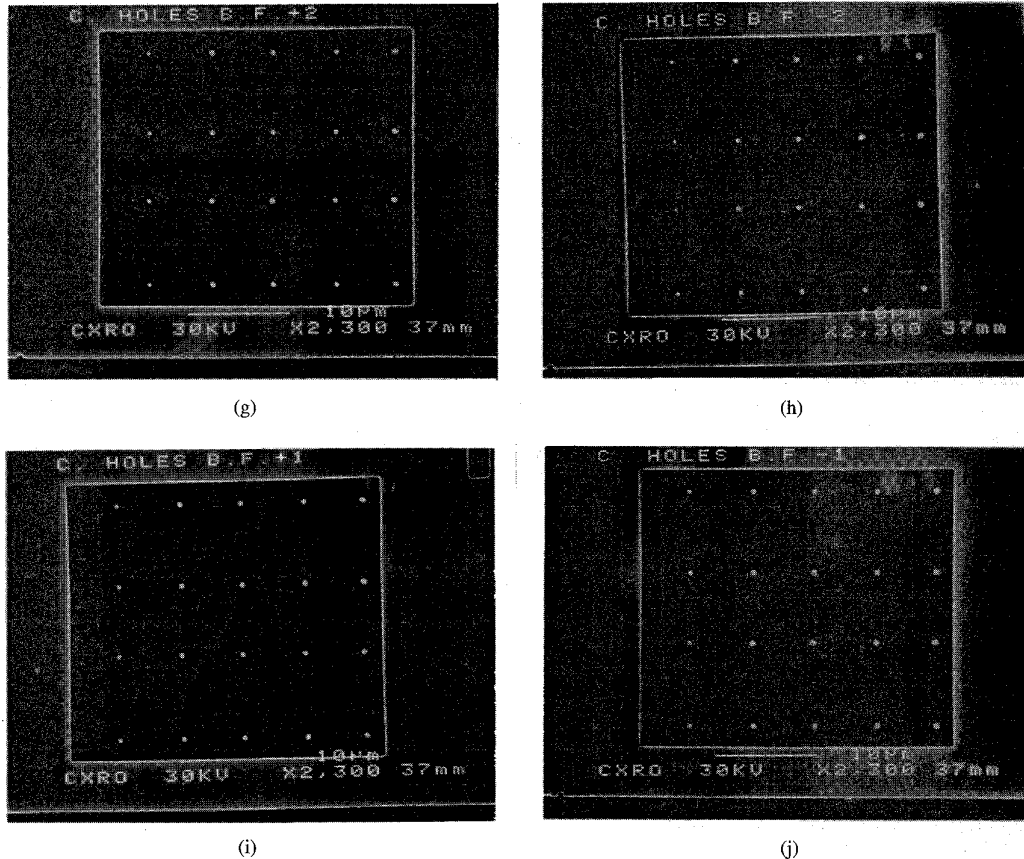Fig. 15 shows the SEM pictures of the resist posts (contact holes) at different defocus plane at

(g)

(h)

(i)

(j)

Fig. 15.   (Continued.)

0.2 μm increment ranging from +1 μm to −1 μm. Specifically, from top to bottom on the left, the pictures correspond to +1.0 μm, +0.8 μm, +0.6 μm, +0.4 μm and +0.2 μm defocus respectively. Similarly, from bottom to top on the right, the pictures correspond to −0.2 μm, −0.4 μm, −0.6 μm, −0.8 μm, and −1.0 μm defocus respectively. In each picture, counting from the left, the first column corresponds to a conventional binary contact hole mask; the second column corresponds to the mask in Fig. 3(b), the third column corresponds to the mask in Fig. 7(a), the fourth and fifth columns correspond to the masks in Fig. 8(a) and (b) respectively.

From now on, we refer to the mask and its corresponding resist image in column n of the SEM pictures as mask n and pattern n, respectively. Since masks 2 and 3 were designed under different numerical aperture and degree of partial coherence from masks 4 and 5, and mask sizes were not scaled to accommodate the differences, it is inappropriate to compare patterns 2 or 3 with patterns 4 or 5. Instead we begin by comparing patterns 1, 2, and 3 with each other, and then move on to comparing patterns 4 and 5 with each other.

Comparing patterns 1, 2 and, 3, our designed phase shift masks 2 and 3 clearly show larger light intensity and longer depth of focus than the binary mask 1. The reason that the asymmetrical mask 2 performs better than the quasisymmetrical mask can be partially justified by noting that enforcing

symmetry constrains our optimization process to the extent that it prevents it from finding the "best" solution. In other words, while the desired pattern is symmetrical, there is no guarantee that enforcing symmetry in the computation for the optimum mask will result in a better solution than not enforcing it.

Comparing patterns 4 and 5, we find our optimized mask resulting in pattern 5 to have a larger light intensity and depth of focus than mask 4 from [7], [8]. The stronger light intensity of pattern 5 suggests that we can increase throughput by reducing exposure time; alternatively if we were to scale the masks down according to λ/NA, pattern 4 may not print while pattern 5 has a good chance of printing.

In summary, phase shift masks designed using our proposed approach perform better than or at least the same as conventional phase shift mask, yet offer the convenience of being easier to manufacture as compared to the masks in [2], [3], [7], and [8] because of larger assisting patterns. One possible drawback of our design is that it contains more data than a conventional mask design; however, results in [5] suggest that this modest increase should not increase the write time in a significant way.

VI. SUMMARY AND DISCUSSION

In this paper, we have proposed a new approach for systematic phase shift mask design. This new approach differs from previous approaches in that the mask is considered to be a

collection of many objects with different phases, sizes and lo-
cations, instead of many pixels with different phases but fixed
sizes and locations. A silent feature of our proposed approach
is that the complexity of the designed masks can be controlled
by pre-specifying the number of objects and minimum feature
size in advance. The "bacteria" algorithm is proposed in order
to avoid the impractically long computation times needed
for the simulated annealing algorithm. New phase shift mask
configurations obtained by this approach are easier to fabricate
than conventional phase shift mask configurations, yet perform
as well or better. A "fair" comparison of computation times
between the bacteria algorithm and the SA algorithm is hard to
define. Our preliminary experience indicates that, for the same
computation domain, and for optimization results with similar
performance, the bacteria algorithm is 10 times faster than the
SA algorithm. More complex mask patterns can be studied
as research efforts continue in this direction. Further research
should be directed to the development of a more sophisticated
"bacteria" algorithm which more or less converges to a near-
global minimum.

ACKNOWLEDGMENT

### REFERENCES

[1] D. M. Newmark and A. R. Neureuther, "Phase-shifting mask design tool," in *BACUS 11th Annual Symp. Microlitho.*, 1991.
[2] Y. Liu and A. Zakhor, "Binary and phase-shifting mask design for optical lithography," *IEEE Trans. Semiconduct. Manufact.*, vol. 5, pp. 138–152, May 1992.
[3] Y. Liu, A. K. Pfau, and A. Zakhor, "Systematic design of phase-shifting masks with extended depth of focus and/or shifted focus plane," in *SPIE Symp. Optical/Laser Microlitho.*, vol. 1674–1602, Mar. 1992.
[4] B. E. A. Saleh and S. I. Sayeh, "Reduction of errors of microphotographic reproduction by optimal corrections of original masks," *Optical Eng.*, vol. 20, pp. 781–787, 1981.
[5] C. Spence, A. Muray, P. Buck, and U. Quinto, "Manufacturing issues for OPC masks," *Preprint*, June 1994.
[6] A. Starikov, "Use of a single size square serif for variable print compensation in microlithography; method, design and practice," in *SPIE Symp. Optical/Laser Microlitho.*, vol. 1088, pp. 34–36, 1989.
[7] T. Terasawa, N. Hasegawa, T. Hurosaki, and T. Tanaka, "0.3-micron optical lithography using a phase-shifting mask," in *SPIE Symp. Optical/Laser Microlitho.*, vol. 1088, pp. 25–33, 1989.
[8] T. Terasawa, N. Hasegawa, T. Tanaka, and S. Katagiri, "Improved resolution of an i-line stepper using a phase-shifting mask," *J. Vacuum Sci. Technol.*, vol. B8, no. 6, pp. 1300–1348, Nov./Dec. 1990.
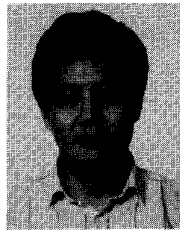
Yong Liu (A'89-S'90-M'91) was born in Yunnan Province, P.R.O.C. He received the B.S. degree in electrical engineering in 1984 from Tsinghua University, Beijing, and the M.S. and Ph.D. degrees from the University of California, Berkeley, in 1989 and 1992 respectively.

In 1992, he joined the Integrated Technology Division, Advanced Micro Devices, Inc., Sunnyvale, CA, doing development work on phase shift mask for optical lithography. In 1994, he managed a software development contract on 3D interconnect parasitic extraction at Sematech, Austin, TX. He is now with CIDA Technology Inc., Sunnyvale, CA, developing tools for layout parasitic extraction. His interests are IC design verification, CMP modeling, substrate noise modeling, optical lithography, telecommunication and signal processing.
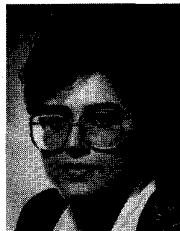
Avideh Zakhor received the B.S. degree from California Institute of Technology, Pasadena, and the S.M. and Ph.D. degrees from Massachusetts Institute of Technology, Cambridge, all in electrical engineering, in 1983, 1985, and 1987, respectively.

In 1988, she joined the faculty at the University of California, Berkeley, where she is currently Associate Professor, Department of Electrical Engineering and Computer Sciences. Her research interests are in the general area of signal processing and its applications to images and video, and lithography. She has been a consultant to a number of industrial organizations, holds four U.S. patents, and is the co-author of the book, "Oversampled A/D Converters" with Soren Hein.

Dr. Zakhor was a General Motors scholar from 1982 to 1983, and received the Henry Ford Engineering Award and Caltech Prize in 1983. She was a Hertz fellow from 1984 to 1988 and has also received the Presidential Young Investigators (PYI) award, IBM junior faculty development award, the 1990 Analog Devices junior faculty development award, and 1992 Office of Naval Research (ONR) young investigator award. She is currently a member of the technical committee for image and multidimensional digital signal processing.
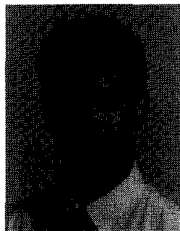
Marco A. Zuniga, received the B.S.E.E. degree from the University of Texas, Austin, in 1991, and the M.S.E.E. degree from The University of California, Berkeley, in 1994. He is currently completing his work for the Ph.D. degree under Prof. A. Neureuther at the University of California, Berkeley.